



CHALMERS

Chalmers Publication Library

Interpreting the Total Isotropic Sensitivity and Diversity Gain of LTE-enabled wireless devices from Over The Air Throughput Measurements in Reverberation Chambers

This document has been downloaded from Chalmers Publication Library (CPL). It is the author's version of a work that was accepted for publication in:

IEEE Access (ISSN: 2169-3536)

Citation for the published paper:

Hussain, A. ; Kildal, P. ; Glazunov, A. (2015) "Interpreting the Total Isotropic Sensitivity and Diversity Gain of LTE-enabled wireless devices from Over The Air Throughput Measurements in Reverberation Chambers". IEEE Access, vol. 3 pp. 131-145.

<http://dx.doi.org/10.1109/ACCESS.2015.2411393>

Downloaded from: <http://publications.lib.chalmers.se/publication/227704>

Notice: Changes introduced as a result of publishing processes such as copy-editing and formatting may not be reflected in this document. For a definitive version of this work, please refer to the published source. Please note that access to the published version might require a subscription.

Chalmers Publication Library (CPL) offers the possibility of retrieving research publications produced at Chalmers University of Technology. It covers all types of publications: articles, dissertations, licentiate theses, masters theses, conference papers, reports etc. Since 2006 it is the official tool for Chalmers official publication statistics. To ensure that Chalmers research results are disseminated as widely as possible, an Open Access Policy has been adopted. The CPL service is administrated and maintained by Chalmers Library.

(article starts on next page)

Interpreting the Total Isotropic Sensitivity and Diversity Gain of LTE-enabled wireless devices from Over The Air Throughput Measurements in Reverberation Chambers

Ahmed Hussain, Per-Simon Kildal, *Fellow, IEEE*, and Andrés Alayón Glazunov, *Senior Member, IEEE*
 Department of Signals and Systems, Chalmers University of Technology, Gothenburg, Sweden

Abstract—The characterization of the performance of wireless devices is the key to developing new RF products conforming to the latest communications protocols. Traditionally, communication performance tests have focused on the RF performance of the tested devices, e.g., smart phones, pads, laptops, etc. More specifically, the focus has shifted from conducted (i.e., cabled) measurements to more realistic Over-The-Air (OTA) characterization of the RF performance of these devices in transmit or receive mode. For example, the receiver performance of 2G and 3G wireless devices can be measured in terms of the total isotropic sensitivity (TIS) that depends on the antenna and the receiver parts of a wireless device. These measurements can be performed in a reverberation chamber setup. However, standard TIS measurements can be time consuming and do not reflect the actual performance gains of Multiple-Input Multiple-Output (MIMO) antenna systems operating over Orthogonal Frequency Division Multiplexing (OFDM) channels, such as those encountered in 4G Long Term Evolution (LTE) systems. Therefore, in order to meet both time and cost efficiency requirements, we propose here a new method to determine the TIS, as well as the diversity performance, of an LTE device based on throughput measurements. The proposed method shows that the TIS of an LTE device is characterized much faster directly from OTA throughput measurements than from standard TIS measurements and with excellent accuracy.

Index Terms—TIS, MIMO, OFDM, LTE, OTA, throughput, reverberation chamber.

I. INTRODUCTION

The Over-The-Air (OTA) performance of wireless devices is of fundamental importance to ensure the overall satisfactory performance of a wireless communication network. Traditionally, in 3GPP, focus has mainly been on the RF characterization of devices. However, the development of new telecommunications standards, such as the Long Term Evolution (LTE), is going towards more complex systems. Hence, there is a need to move the OTA testing focus from RF performance to a more comprehensive approach that looks at performance metrics reflecting system performance.

For 2G and 3G wireless systems the down-link device performance is characterized in terms of their Total Isotropic Sensitivity (TIS) [1] (or sometimes also called Total Radiated Sensitivity (TRS) [2]). A procedure for measuring TIS was developed for anechoic chambers and only for single-port wireless devices in Single-Input Single-Output (SISO)

systems. It involves measuring several value of the sensitivity under stationary conditions, i.e., for several fixed antenna orientations, and for a single incident wave impinging at the antenna. Hence, at each fixed orientation, the measurements in the anechoic chambers are performed under the Additive White Gaussian Noise (AWGN) channel assumption. They are repeated for many different angles of arrival (AoA) of the wave on a pre-defined spherical surface grid. The TIS is then computed as the harmonic mean (i.e, an inverse averaging) of the sensitivity values for the different AoAs [1].

Currently, conducted measurements for conformance tests of Long Term Evolution (LTE) device have been defined in terms of *reference sensitivity levels* specified for different Evolved Universal Terrestrial Radio Access (E-UTRA) frequency bands [3]. However, there is no similar metric, nor a corresponding measurement method, available to determine the OTA receiver sensitivity of 4G wireless devices, e.g., LTE device. Hence, there is a need to fill this gap in order to properly characterize the positive effects of both Multiple-Input Multiple-Output (MIMO) and Orthogonal Frequency Division Multiplexing (OFDM) to overall system performance. This will in turn facilitate sorting out the good performing device from the bad performing device as well as sorting out the good antenna designs from the bad antenna designs both of them from a system performance point of view.

It is well-known that a reverberation chamber emulates the Rich Isotropic Multipath (RIMP) environment if it is well-stirred [4], where the term “rich” means many incoming waves, typically more than 100, and isotropic means that the Angles-of-Arrival (AoA) of the incoming waves are uniformly distributed over the unit sphere. More specifically, isotropy shall be understood here as the uniform distribution of the AoAs obtained as a result of the averaging over several positions of the stirrers in the reverberation chamber. These properties of the emulated channel have, among other things, contributed to their widespread use for OTA testing in recent years [5], [6]. The total radiated power (TRP) and the TIS have been successfully measured for 2G and 3G wireless devices [7], [8]. The TIS measurement setup was later extended into testing throughput of WLAN devices [9]. It has been shown through extensive measurements that reverberation chambers provide accurate and cost-efficient alternatives for the OTA characterization of antennas in terms of the antenna efficiency,

the diversity gain [10], and the maximum available MIMO capacity [11]. In addition, many practical small multi-port antennas such as the multi-wideband handset antenna in [12], and a decade bandwidth multi-port antenna with feeding network in [13] have been successfully designed through OTA characterization in a reverberation chamber. These passive measurements were in good agreement with corresponding measurements done in anechoic chambers [14]. It has been shown that the reverberation chamber is an accurate tool for measuring radiation efficiency of antennas, and there exist a good Rician-factor-based model for the uncertainty given in [15]. In addition, there has been observed really good agreement between theoretical models and measurements for MIMO and OFDM enabled LTE devices [16], [17]. Recently, good agreement between simulations and measurements in reverberation chambers has also been shown for a mockup of a multiport LTE phone in different talk positions in terms of diversity gain [18].

Despite the versatility of reverberation chambers, the TIS measurements of 2G and 3G devices are relatively time consuming. This is because measurements are repeated at many, e.g., 800 or more, stationary stirrers positions for different realizations of the AWGN channel [8]. This takes much longer time than doing OTA throughput measurements, during which the stirrers are moved continuously. Previously, it has been proposed to measure the receiver quality during continuous stirring/fading, referred to as average fading sensitivity (AFS). However, this approach was developed for 2G and 3G systems for which cases there are no simple relations between the TIS and the AFS. This may be explained by irreducible bit errors occurring at large r.m.s. (root mean squared) delay spreads and resulting channel fading over the transmit signal bandwidth. In contrast, in 4G, the transmit signal bandwidth of each communication channel is divided in several sub-channels that are combined constructively on the receiving side by means of the OFDM. Thus, the 4G system can accept much larger r.m.s. delay spreads (and equivalently smaller coherence bandwidths) than earlier systems [19].

In this paper we make use of the simple, yet useful, ideal threshold receiver model [17]. The threshold receiver model allows to determine the throughput including array gain, antenna diversity gain and frequency diversity gain of a wideband MIMO antenna system operating across the OFDM sub-channels [16]. The coherence bandwidth is controlled by loading the chamber with absorbers [21]. Simulations are performed based on simplified flat- and frequency-selective fading channel models based on the system bandwidth and coherence bandwidth. The analysis is based on measurements performed on single bit stream for a SISO system and a 2×2 MIMO system in diversity mode. Generally, the throughput performance corresponds to the probability of detection (PoD) of the measured bitstream.

The contributions of this paper are summarized as in the four points below, where we use the term TIS to describe the receiver sensitivity measured according to the above-mentioned standard procedure for 2G and 3G systems, in reverberation chambers:

- We show that the TIS does not reflect the actual perfor-

mance improvement provided by the OFDM.

- We present a new approach to estimate TIS in OFDM MIMO channels from throughput measurements. This is done by using pre-defined look-up values of the PoD (i.e., relative throughput). These PoD levels are obtained from theoretical channel models assuming independent and identically distributed (i.i.d.) complex Gaussian channels and uncorrelated 100% efficient antennas.
- The proposed method will provide much faster measures of the receiver sensitivity since throughput measurements are performed on a continuous basis as opposed to corresponding standard TIS measurements.
- The throughput measurements provide, clearly in addition to throughput, a complete characterization of the performance of MIMO-OFDM enabled LTE device, in terms of TIS and diversity gain due to the use of multiple frequency sub-channels (i.e., OFDM) and multiple antenna ports (i.e., MIMO).

It is worthwhile to note that the proposed OTA measurements of the receiver sensitivity (of 4G devices obtained by means of OTA throughput) inherently include the impact of the most significant factors contributing to the performance of the wireless device. For example, the quality of the receiver, the effect of noise and interference, the antenna efficiencies, the correlation between the antenna ports, the processing algorithms behind MIMO and OFDM, and other digital features are readily identified and can be used to interpret the quality associated with each of them.

The remainder of the paper is organized as follows: Section II introduces the threshold receiver model, the OFDM channel fading model and the maximum ratio diversity combining of the antennas and sub-channels; Section III provides a description of the conducted and OTA measurement setup and the description of the standard TIS definition for SISO and MIMO devices, and the definition of TIS of the proposed throughput-based estimation approach; Section IV provides measurement results for conducted receiver sensitivity and throughput, measurement results for standard OTA measurements of TIS and throughput as well as TIS and diversity gain estimated from throughput measurements based on the threshold receiver model; Section V provides a comparison between standard and throughput-based TIS estimation; Section VI provides additional results and discussions on throughput and TIS measured at different frequency bands, and throughput for the same device measured with internal antennas. Conclusions are given in Section VII.

II. RECEIVER MODEL, CHANNEL FADING MODEL AND DIVERSITY COMBINING ALGORITHMS

For the sake of completeness of exposition we briefly present the ideal threshold receiver model introduced in [17]. We present also the basic channel model used to account for the frequency-selective fading nature of the channel (see, e.g., [22] for other more advanced channel models for LTE systems). Both models have been verified to be in good agreement with the OTA reverberation chamber measurement

method. Results presented further in this paper add to existing results.

A. Digital threshold receiver model

First, let's assume that the received signal at the device antenna port is constant, but it may be corrupted by AWGN (Additive White Gaussian Noise). This is typically the case for *conducted measurements* used in conformance testing of wireless communication systems [2]. In this case, the performance of the device is measured by connecting it, by means of cables, to a communication tester emulating a base station operating at the corresponding communication protocol, e.g., LTE. The throughput TPUT is then modelled in the conducted measurements case as

$$\text{TPUT}(P) = \text{TPUT}_{\max} \begin{cases} 0 & \text{when } P < P_{\text{th}} \\ 1 & \text{when } P \geq P_{\text{th}} \end{cases}, \quad (1)$$

where P is the power available at the signal port of the receiver, P_{th} is the threshold level, TPUT_{\max} is the maximum throughput achievable given the operational modulation, coding and bandwidth. The ideal threshold receiver model is based on the basic assumption that in the AWGN channel the receiver will detect all groups (e.g., blocks) of bits correctly as long as the received power P is larger than a certain threshold, and that the communication link breaks down completely when the received power is below this threshold. Hence, the Block Error Rate (BLER) will increase immediately to 100% when the received power P becomes lower than the threshold level P_{th} . Correspondingly, the percentage of correctly detected bits will immediately drop from 100% to 0%. The resulting throughput TPUT will be a step function from minimum to maximum when plotted against increasing values of P .

Secondly, let's assume that the device is operated in a fading environment, i.e., the power at the signal port of the receiver varies severely due to destructive and constructive interference of multipath components as in, e.g., RIMP. This is typically the case for *OTA measurements* both in laboratory conditions and in the real channels. In this case, the observed throughput variations will be much greater around the threshold as compared to the AWGN channel. This variation is characterized by the CDF (cumulative distribution function) of the channel. It can be seen, that the relative throughput is equal to counting the number of times the instantaneous power of the received power is above the threshold, compared to the total number of observations. In practice, averaging over all the possible fading states, the relative *average throughput* equals the *Probability of Detection* (PoD), i.e., the *complementary CDF* (or CCDF) of the outage probability. This can be expressed as

$$\begin{aligned} \text{TPUT}_{\text{av}}(P_{\text{av}}) &= \text{TPUT}_{\max} \text{PoD}(P_{\text{av}}/P_{\text{th}}) \\ &= \text{TPUT}_{\max} \{1 - \text{CDF}(P_{\text{th}}/P_{\text{av}})\}, \end{aligned} \quad (2)$$

where P_{av} is the average received power available at the device signal port, and the CDF describes the cumulative distribution function of the received signal level. The CDF represents probability of outage, whereas the PoD represents the complementary probability, if $\text{PoD} = 0.9$ (i.e., 90% CCDF-level) then $\text{CDF} = 0.1$ (i.e., 10% CDF-level).

Different algorithms are usually implemented in the receiver to mitigate, or to take advantage of fading effects. Single or multiple bitstreams are then processed to provide the desired throughput. The CDF describes the distribution of the processed signals. Thus, the OTA throughput can be estimated in RIMP from the threshold receiver theory if we know the algorithms behind MIMO and OFDM.

B. Flat-fading and frequency-selective channel model

In this paper we consider the RIMP channel since it is the channel emulated in well-stirred reverberation chambers [23]. Hence, the received power available at a port of the device antenna can be described by the exponential distribution (with Rayleigh distributed voltages and complex Gaussian distributed complex voltage vectors) at a single frequency. This type of distribution remains the same also regardless of frequency within the considered system bandwidth B_s . The frequency-selectivity is modeled in terms of OFDM frequency sub-channels in relation to the coherence bandwidth of the channel B_c . The frequency-selectivity is determined by the ratio B_s/B_c , i.e., the channel is said to be flat-fading or frequency non-selective if $B_s/B_c \leq 1$ and frequency-selective in the opposite case or rather if $B_s/B_c \gg 1$.

The frequency-selectivity determines the correlation between adjacent frequency components of the received signal within the whole bandwidth of interest, e.g., in this paper we use the 0.5 level of the frequency auto-correlation function as the defining point for the coherence bandwidth. The relative number of uncorrelated frequency bands is then computed as

$$N_{\text{fd}} = \text{NINT} \left(\frac{B_s}{B_c} \right), \quad (4)$$

where $\text{NINT}(x)$ is the function producing the nearest integer of its argument x .

C. Maximum Ratio Combining

The device performance is characterized, in this paper, in terms of the Maximum Ratio Combining (MRC) algorithm. The combining is assumed to take place across the N_r ports of the device antenna, across the N_t antenna ports of an emulated transmitter and across the uncorrelated frequency bands N_{fd} . The MRC adds the signals coherently, which corresponds to adding the powers across the $N_{\text{fd}} \times N_{\text{ant}}$ diversity branches, where $N_{\text{ant}} = N_t \times N_r$ is the total number of antenna links. Indeed, we assume that the OFDM ideally corresponds to using N_{fd} independent MRC-combined diversity channels that are uncorrelated over frequency. In a $N_t \times N_r$ MIMO antenna system the power of the output of the threshold receiver voltage is then modelled as, [20]

$$P = \frac{\sum_{i=1}^{N_r} \sum_{j=1}^{N_t} \sum_{k=1}^{N_{\text{fd}}} P_{ijk}}{N_t N_{\text{fd}}}, \quad (5)$$

where P_{ijk} is the power at each received antenna port i due to transmit antenna port j and OFDM sub-channel k ; N_r and N_t are the number of received and transmit antennas, respectively. It is worthwhile to note that, here, we characterize the frequency selectivity in terms of the ratio of the system

bandwidth and the coherence bandwidth. If the whole channel over the system bandwidth is flat, then the sub-channel will also be frequency flat. If the whole channel is frequency selective, then, the channel is subdivided in a number of flat-fading channels in our simplified model. According to the channel model assumption above all realizations of P_{ijk} are i.i.d. exponentially distributed variables. In this paper, we consider the SISO and the 2×2 MIMO cases.

III. MEASUREMENT SETUPS AND METHODS

The employed setups for measuring the TIS, the throughput and the corresponding receiver sensitivity of the Device-Under-Test (DUT) are shown in Fig. 1. The measurements were performed in the Bluetest RTS60 reverberation chamber described in detail in [15]. The TIS and throughput measurement setups and device settings are essentially the same in both the conducted and the OTA measurements. The same settings on the base station regarding modulation and coding scheme, system bandwidth, frequency band, and transmission mode. The conducted measurements have no delay spread, whereas it was controlled in the reverberation chamber by loading the chamber to a specific time delay spread. The calibration of the cable losses is the same in both cases. The average power transfer loss of the reverberation chamber must be included by using a reference antenna with known radiation efficiency. The difference in the measurement procedures is explained in the following subsections.

The DUT is a commercial LTE device, i.e., the Huawei E398 as shown in Fig.1. Typically, it is used as a mobile 4G USB dongle providing internet connection to a computer or a laptop. It is a two-port receiver terminal with an option to connect external antennas to it. The DUT is measured in two different modes, i.e., the SISO mode and the 2×2 MIMO spatial diversity mode. Two external high efficiency discone antennas were connected to the DUT as shown in Fig.1. The main measurements in this paper were performed on the LTE band 7, downlink channel 3100 (uplink: 2535 MHz, downlink: 2655 MHz), Modulation and Coding Scheme Index (MCSI) 19, QAM 64, LTE system bandwidths of 5, 10, 20 MHz. The emulated channel coherence bandwidths are equal to 3, 9, and 18 MHz with corresponding channel delay spreads of 210, 60, and 30ns, respectively. The relation between the coherence bandwidth and the time delay spread is given in [21].

The LTE base station simulator used to communicate to the DUT is an Anritsu MT8820C Radio Communication Analyzer. The modulation and coding scheme were kept fixed, while the base station is swept through a range of transmit powers. In real-life, the modulation and coding scheme is adaptive and not fixed. However, at the time of writing this article there was no such base station simulator available which could provide this feature. Therefore, we need to know performance for fixed settings in order to understand the measured results. Such data will also be needed for an operator in order to make appropriate resource allocations to different users.

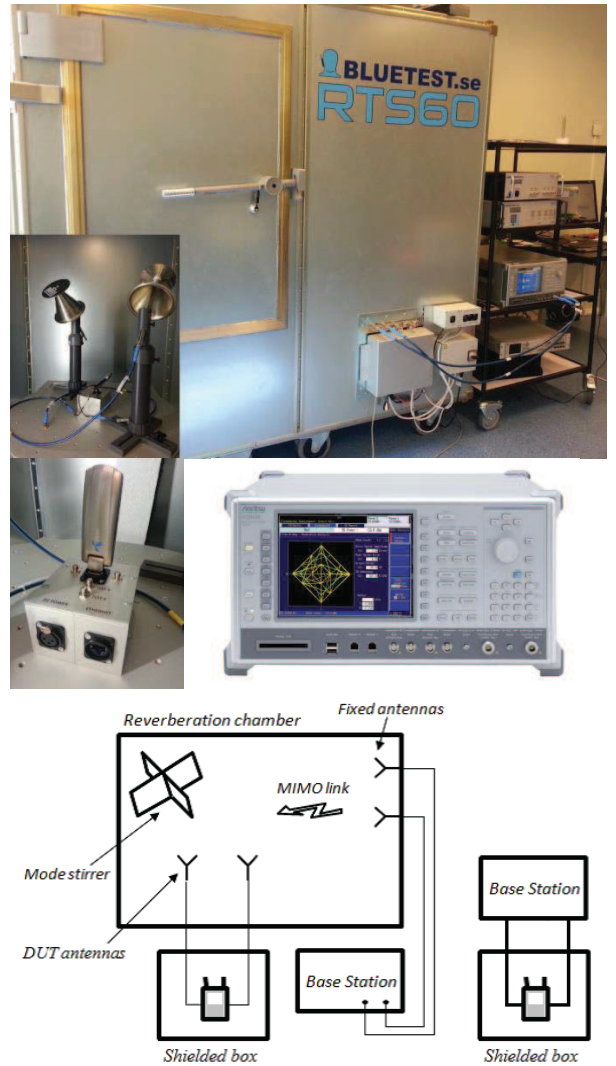


Fig. 1. Measurement setup of TIS and throughput measurements. The photos (upper) show LTE base station emulator connected to DUT with external antennas located inside reverberation chamber; the DUT inside the chamber; and the LTE base station emulator. The drawing (lower-left) schematically shows the complete OTA measurement setup. The drawing (lower-right) shows the conducted throughput measurement setup.

A. Conducted receiver sensitivity and throughput measurements

Conducted receiver sensitivity measurements are performed by connecting a cable directly between the base station simulator and the DUT, in which case the receiver's so-called *conducted throughput* is measured. The conducted measurement setup is illustrated in the bottom right drawing in Fig.1. The value of P_{th} is found by lowering the signal power level from the base station until BLER suddenly reaches to 100%. The value of P_{th} depends on the receiver hardware as well as the software definitions and settings on the base station. In other words, P_{th} defines the receiver sensitivity of the terminal, which depends on all the components of the RF-chain, as well as the software definitions including algorithms for error correction, modulation and coding schemes, and system bandwidth. The threshold measured using the conducted measurement setup does not include the effect of the antenna.

B. Standard TIS measurements

The SISO TIS performance is commonly quoted for wireless devices and represents the minimum signal power needed to establish a reliable OTA communication link, when using a single receive antenna. The TIS is defined as the average sensitivity of the receiver to a single incident wave when its angle of arrival (AoA) is uniformly distributed over the sphere of unit radius, i.e., a 3D-uniform AoA distribution. The TIS value is measured at a specific BLER, e.g., typically at the 1% BLER, as defined by the standards [1]. In an anechoic chamber the TIS is obtained in a similar way as in conducted measurements and OTA measurements. The signal power from the base station is gradually lowered from the maximum until the BLER reaches the chosen BLER for each AoA. The inverse of this signal power is then weight-averaged over all AoAs to obtain the TIS value of the receiver [1]. The TIS can be deduced from the receivers conducted sensitivity and the total radiation efficiency of the antenna, [1]

$$\text{TIS}_{\text{AC}} = \frac{P_{\text{th}}}{e_{\text{rad}}}, \quad (6)$$

where we have used the subscript AC to indicate that this is the definition used for standard SISO measurements in anechoic chambers. Furthermore, (6) is the *standard definition* of TIS. In practice, the TIS may also be affected by interference and related noise from other components on the DUT [27]. For example, a mobile phone antenna can pick up noise from the memory and the screen of the terminal [28]. Therefore, the TIS may be higher than the conducted sensitivity divided by the total radiation efficiency of the antenna due to added noise at the DUT receiver.

When measuring TIS in the reverberation chamber, the stirrers inside the chamber are static, i.e., they remain at fixed positions while the base station is searching for the required BLER by sweeping through a range of power-levels. The power-level $P_{\text{inst},n}$ at which the required BLER occurs is recorded. This procedure is repeated at many different stirrer positions N_{sp} (e.g., 800 stirrer positions) in the reverberation chamber to get an accurate enough TIS value. This means that the channel is constant while measuring TIS, i.e., the channel is static.

In the Bluetest RTS60 chamber there are two plate stirrers, i.e., one moving in the horizontal direction and another in the vertical direction. The platform stirrer where the DUT is located, is rotated in steps around its vertical axis. A multiport antenna switch is connected between the base station and a multiport transmitting antenna inside the chamber. This switch is used to connect the base station signal successively to each of the three transmitting antenna ports. The fields radiated by the three antennas are orthogonally polarized. Different combinations of these stirrer positions and ports create different static multipath environments due to different constructive and destructive interference of waves inside the chamber. Hence, the instantaneous received power at the DUT antenna can be expressed as a product of three factors: the radiation efficiency e_{rad} of the antenna on the DUT, the average received power $P_{\text{av},n}$ on a reference antenna with 100% efficiency, and a factor accounting for the variation

around the average of the received power for different stirrer positions in the chamber, i.e., the multipath fading. Therefore, for stirrer position number n we can write

$$P_{\text{inst},n} = e_{\text{rad}} P_{\text{av},n} G_{\text{fading},n}, \quad (7)$$

where the $P_{\text{av},n}$ is basically, per definition, the ‘‘TIS’’ at position n of the stirrers and the factor $G_{\text{fading},n}$ accounting for the fading variation around the average of the received power. Then, to obtain the TIS, the harmonic-mean of all the recorded sensitivity levels at each stirrer position n is computed according to

$$\text{TIS}_{\text{RC}} = \frac{N_{\text{sp}}}{\sum_{n=1}^{N_{\text{sp}}} \frac{1}{P_{\text{av},n}}}, \quad (8)$$

where we have used the subscript RC to indicate that this is how the TIS is computed from standard measurements in reverberation chambers. $P_{\text{inst},n}$ is not known due to the random fluctuations (i.e., fading) of the field impinging at the DUT antenna. However, the equivalent received power at which the required BLER is achieved must satisfy $P_{\text{inst},n} = P_{\text{th}}$, i.e., the threshold power, which is independent from the stirrer position n . Under this condition we may insert $P_{\text{av},n} = P_{\text{th}}/e_{\text{rad}}G_{\text{fading},n}$ in (8). After straightforward algebraic manipulations we immediately arrive at (6), where we use that the average of the fading component is one, i.e., $\sum_{n=1}^{N_{\text{sp}}} G_{\text{fading},n} = N_{\text{sp}}$. Hence, the SISO TIS defined for the anechoic chamber (see (6)), i.e., in a static field and the TIS defined for the reverberation chamber (see (8)), i.e., in a fluctuating field are then equivalent since both correspond to average receive sensitivity in an isotropic or 3D-uniform field distribution. It is worthwhile to note that, in practice, the transition over the threshold level is rather steep that it does not really matter much at which BLER-level we read it.

The relationship (6) applies to SISO OFDM (flat-fading as well as frequency-selective channels) as long as the number of fading OFDM frequency sub-channels are chosen equal to the number of uncorrelated frequency bands (4), the instantaneous received power (7) at the stirrer position n is the sum of N_{fd} MRC signals over the uncorrelated frequency sub-channels according to (5). The embedded radiation efficiency of the antenna must be the same at each sub-channel and the average power at each sub-channel is also the same. It is worthwhile to note that the MRC algorithm has shown good agreement with measured effects of OFDM in [16], [17]. However, when we use other diversity combining algorithms than MRC, such as selection combining, the simple relation (6) is not valid anymore even when the conditions stated above are satisfied. Then, the simulated value of TIS becomes higher, i.e., the receiver sensitivity becomes worse.

For the MIMO case in the diversity mode, the relationship (6) is valid for MIMO OFDM (flat-fading as well as frequency-selective channels) if the above conditions are satisfied for each of the identical $N_t \times N_r$ MIMO links. Moreover, in practice, the received power of an actual DUT with N_r receive antennas will have to be normalized by N_r in (5) since the corresponding number of channels will be combined at the receiver. The measured TIS of a $N_t \times N_r$ MIMO system is then

TABLE I. Simulated MIMO-OFDM diversity gains for i.i.d. cases: 1×1 SISO & 2×2 MIMO systems with different orders of frequency diversity

N_{fd}	1	2	3	4	7	∞	1	2	3	4	7	∞
$N_t \times N_r$	1×1	2×2										
DG _{A-G} , [dB]	0	0	0	0	0	0	3	3	3	3	3	3
DG _{F-D} , [dB]	0	3.8	5.3	6.0	7.1	9.6	0	1.2	1.7	2.1	2.5	3.6
DG _{MIMO-D} , [dBR]	0	0	0	0	0	0	6	6	6	6	6	6
DG _{0.90} , [dBR]	0	3.8	5.3	6.0	7.1	9.6	9.0	10.2	10.7	11.1	11.5	12.6
PoD(1), [%]	36	40	43	43	45.5	0 – 100	43.5	45.2	46.5	47.2	48	0 – 100

improved by a factor N_r relative to a SISO system under the same conditions. Hence, in this ideal case the TIS (measured according to the standard TIS procedure) becomes

$$\text{TIS} = \frac{P_{th}}{e_{rad} N_r}, \quad (9)$$

where P_{th} is the conducted receiver sensitivity level for the MIMO case.

C. Extracting TIS from OTA throughput measurements

As we have shown in the introductory section, the OTA throughput performance of GSM, WCDMA, LTE and WiFi devices in RIMP can be easily measured using an appropriate base station emulator and a reverberation chamber. In contrast to TIS measurements, throughput measurements can be performed using faster and easier procedures. Indeed, during throughput measurements, the stirrers in the reverberation chamber are continuously moving to provide a continuous fading environment. The data from the base station simulator is sent through the emulated fading channel in the reverberation chamber to the LTE DUT. The DUT sends back positive acknowledgement (ACK) for the correctly received data and negative acknowledgement (NACK) for erroneous data. The throughput (or similarly the Probability of Detection) is then simply calculated at the base station from the received ACKs and NACKs. This is repeated many times, e.g. by sending 200 blocks of data 1000 times for each average power-level in a fading sequence, to get good accuracy of the throughput.

In practice, it is desired to perform time-efficient and cost-efficient measurements. Hence, a new method based on throughput measurements can be devised on the average throughput expressed through the probability of detection (2). Given the relationship between TIS and conducted receiver sensitivity P_{th} (6), we see that $\text{TIS} = P_{th}$ for a 100% efficient antenna on the DUT (It is worthwhile to note that we have dropped the subscript in (6) to highlight that we are using the standard definition of TIS). From (2) we can then obtain the relative throughput level at which $P_{av} = P_{th} = \text{TIS}$

$$\frac{\text{TPUT}_{av}(\text{TIS})}{\text{TPUT}_{max}} = \text{PoD}(1), \quad (10)$$

where $\text{PoD}(1)$ is the probability of detection at TIS for 100% efficient antennas operating under a pre-defined MIMO OFDM diversity algorithm. In this paper we assume the model presented above in Section II.B and Section II.C. From this model the probability of detection curves are obtained and hence $\text{PoD}(1)$ can be determined too. The values of the

probability of detection in (10) will be different for a different number of uncorrelated frequency sub-channels, the number of transmit and receive antennas and other system parameters in general.

Now assuming we have performed calibrated OTA throughput measurements on the DUT, we can obtain an estimate of the TIS using relation (10)

$$\hat{\text{TIS}} = \text{TPUT}_{av}^{-1} \left(\text{TPUT}_{max} \text{PoD}(1) \right), \quad (11)$$

where $\text{PoD}(1)$ is the relative throughput (10) obtained from the threshold receiver model and the OFDM channel fading model and the MRC MIMO diversity model explained in Section II. TPUT_{max} and TPUT_{av} are the measured maximum throughput and the measured average throughput (is a function of the average received power), respectively. TPUT_{av}^{-1} denotes the inverse function of TPUT_{av} . In this case, taking the inverse corresponds to reading the received average power at the CCDF level given by $\text{PoD}(1)$. The values of $\text{PoD}(1)$ can be provided in a table form for each sets of coherence bandwidth B_c , system bandwidth B_s , number of transmit antennas N_t and receive antennas N_r .

It is worthwhile to note that the estimated TIS (11) does include the actual embedded antenna efficiency of the DUT antennas and is, in general, a measure of the DUT in receive mode including the performance of the antenna.

D. Extracting the diversity gain from OTA throughput measurements

The antenna diversity gain is usually defined at the 1% CDF level [10]. The TIS is normally defined at 1.2%, 2%, or 5% BLER [1]. These values correspond to PoDs at 98.8%, 98%, and 95%. However, the PoD curve is not so easy to measure accurately at these high PoD levels, so it is better to define the gains of the PoD curves at the 90% or the 95% levels. We here choose to define the gain at the 90% PoD level. The simple relationship between PoD and CDF is the given by (see (2) and (3))

$$\text{PoD}(P_{av}/P_{th}) = 1 - \text{CDF}(P_{th}/P_{av}), \quad (12)$$

Hence, the diversity gain of an OFDM MIMO MRC diversity scheme relative the narrowband SISO channel can be expressed as follows

$$\text{DG}_{0.90} = 10 \log_{10} \left(\frac{\text{PoD}_{N_t \times N_r \times N_{fd}}^{-1}(0.90)}{\text{PoD}_{1 \times 1 \times 1}^{-1}(0.90)} \right), \quad (13)$$

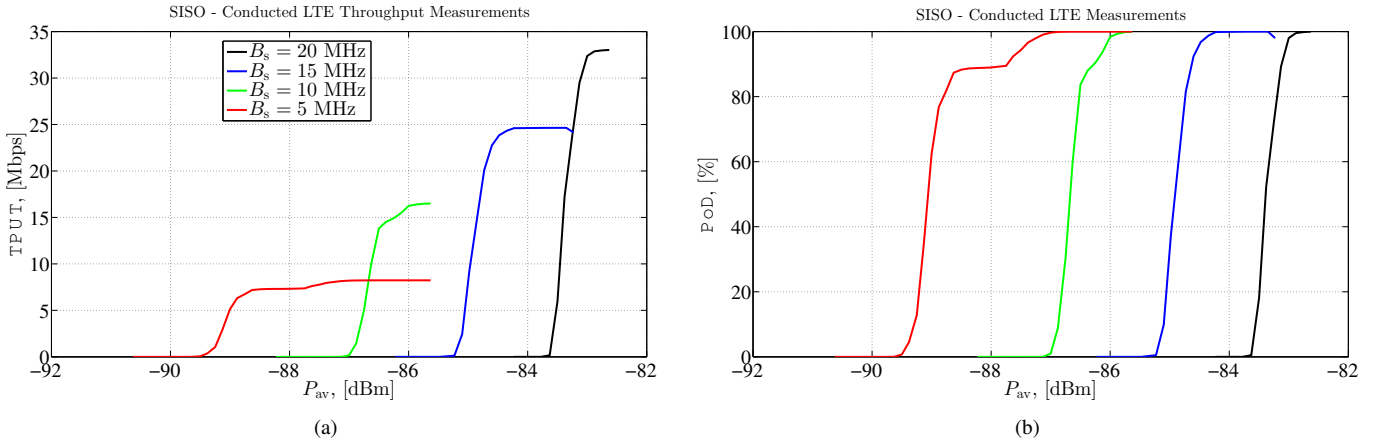


Fig. 2. Measured conducted throughput (a) and corresponding probability of detection (b) of LTE device with cable between its antenna port and the LTE base station emulator for different system bandwidths ($B_s = 20, 15, 10, 5$ MHz).

where the subscripts have been used to highlight the fact that the probabilities of detection are different functions depending on N_t , N_r and N_{fd} . From the OFDM MIMO MRC diversity model (5) it can be shown that the total diversity gain can be expressed as

$$DG_{0.90} = DG_{A-G} + DG_{MIMO-D} + DG_{F-D}, \quad (14)$$

where the diversity gain defined in this way includes both the effects of the antenna diversity through the array antenna gain $DG_{A-G} = 10 \log_{10}(N_r)$ and the MIMO diversity gain $DG_{MIMO-D} = 10 \log_{10}(N_r N_t)$ as well as the OFDM in terms of a so called frequency diversity gain $DG_{F-D} = f(N_{fd})$. The latter term can be derived from numerical simulations where the frequency diversity gain is compared to the same $N_t \times N_r$ MIMO system in a flat fading Rayleigh channel with $N_{fd} = 1$.

IV. RESULTS AND ANALYSIS

In this section we present both numerical simulations and measurement results obtained using the models, the characterization methods and measurement setups described above.

A. Conducted receiver sensitivity and throughput

The measured conducted throughput of the LTE DUT shows a clear threshold in the throughput curves. This behaviour is clearly observed at all the considered LTE system bandwidths as shown in Fig. 2. We see that the measured threshold is quite close to being ideal; however, as explained above, the impact of noise can be clearly observed. As can be seen, the BLER changes from 0% to 100% over a small change of P_{av} around the threshold level P_{th} . The 3GPP defines a *reference sensitivity levels* as the power required to achieve the 95% of the maximum conducted throughput. At 5 and 10 MHz LTE system bandwidths, denoted by the red and the green curves, respectively, a shoulder in the throughput curve can be observed. Hence, the receiver sensitivity may vary ± 1 dB depending on the definition used.

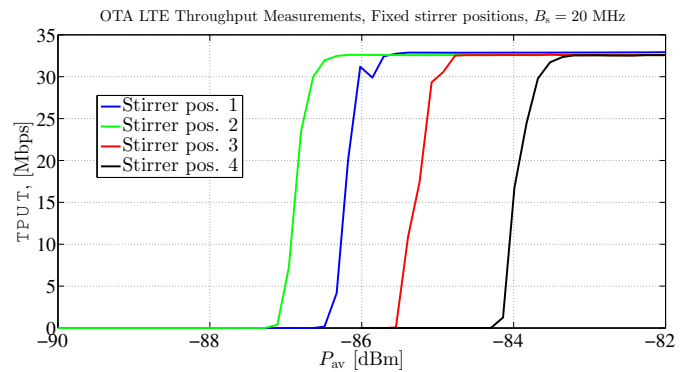


Fig. 3. Four measured throughput curves of an LTE device for the standard TIS measurements. Each curve corresponds to different fixed stirrer position inside the reverberation chamber.

B. Standard TIS and throughput

Measurements were performed in the reverberation chamber following the standard TIS measurement procedure explained above (in Section III.B) by selecting the configuration settings on the LTE base station simulator as described in Section III. We performed throughput measurements for different fixed stirrer positions in reverberation chamber. Then, we observed that each throughput curve shows a clear threshold, in the same way as for the conducted case. However, the instantaneous threshold level at the 1% BLER of each of these curves appears to be different as shown in Fig. 3 for four arbitrarily chosen stirrer positions. The TIS in the reverberation chamber is then obtained from (8). In order to illustrate this behaviour more in detail than results shown in Fig. 3, we simulate the ideal threshold receiver in SISO Rayleigh fading channels for $N_{fd} = 1$ and $N_{fd} = 7$ as shown in Fig. 4a and Fig. 4b, respectively. The step-function throughput curves (blue lines) represent many different ideal instantaneous thresholds for a Rayleigh distributed SISO channel. The abscissa represents the average received power level. Thus, $N_{fd} = 1$ and the variation of the observed thresholds is given by the exponential distribution of the instantaneous received power-level at the DUT.

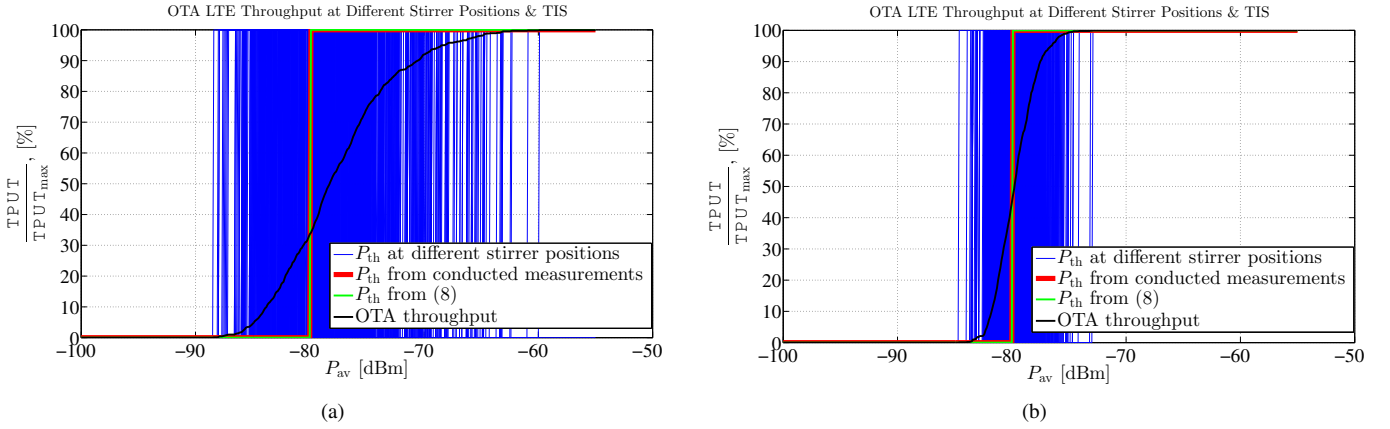


Fig. 4. Modeled P_{th} (blue lines) for a SISO system at different stirrer positions of reverberation chamber in frequency-flat fading by using the ideal threshold receiver model and TIS (green line) using equation (8). The cases of $N_{fd} = 1$ and $N_{fd} = 7$ OFDM sub-channels are depicted in (a) and (b), respectively.

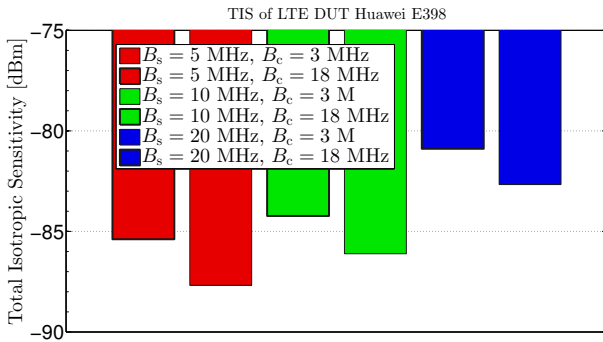


Fig. 5. Measured TIS of a commercial LTE device for different system bandwidths and coherence bandwidths for SISO case.

For the SISO case with $N_{fd} = 7$, the modeled thresholds are much closer together than the case with $N_{fd} = 1$. This is due to the difference in the MRC fading distribution as the number of combined frequency sub-channels increases. Thus, the OFDM reduces the power level fluctuations due to the fading resulting in a fading gain.

The obtained TIS values are shown in Fig. 5. The obtained TIS values are just slightly larger than the conducted receiver sensitivity levels since the two external disccone antennas are highly efficient. The TIS is expected to be larger than the receiver sensitivity as shown by the relationship (6). We also see that as in the case of the conducted measurements the receiver sensitivity becomes worse, i.e., TIS becomes larger, as the system bandwidth increases. Furthermore, as explained in Section III, we expect the TIS to be independent from the OFDM frequency diversity under the given model assumptions. Indeed, it is expected that the TIS will remain the same at different ratios B_s/B_c (i.e., independently of the number of uncorrelated frequency sub-channels) while keeping the system bandwidth B_s constant. However, we see that the TIS gets worse (i.e., increases) as B_s/B_c increases for a fixed B_s . However, this behaviour seems to be systematic and cannot be explained by the measurement uncertainty alone. A plausible explanation could be that the algorithms built into the devices

are different for different providers, or that the antennas have very different impedance mismatch factor in different OFDM sub-channels. However, under the assumptions we've made above, the OFDM algorithm should not have any effect on the TIS performance if extracted properly. Moreover, the TIS alone does not provide any further information regarding the performance of the MIMO OFDM MRC diversity scheme. Therefore, TIS obtained from the standard measurement approach seems not to be a good performance measure of the reception quality of the LTE device in this case. Next, we present results for the new proposed approach to estimate TIS.

C. Throughput measurements and derived TIS

As we explained in Section II above, the throughput curve presented relative to its maximum on a scale between 0 and 1 represents the probability of detection of transmitted information blocks (see (2)). This interpretation reflects the situation when the DUT in any position inside the chamber either detects the bitstream, or it doesn't. There is ideally nothing in between, as a result of the threshold receiver. Therefore, we can simply count the number of detections. This number relative to the total number of attempts to detect the bitstreams becomes the PoD. The PoD makes it possible to generalize the continuous throughput measurement approach to a step-by-step procedure over stationary stirrer positions. And, then we can even consider the PoD in practice being taken over a distribution of different devices of different users in space or the distribution of the different orientations and positions of the device of a single user. *In reverberation chambers we have PoDs in RIMP, but we can also use this approach to characterize performance in other environments.*

To illustrate the above we have simulated the conducted SISO throughput and the SISO OTA throughput for different orders of frequency diversity, $N_{fd} = \{1, 2, 3, 4, 7, 100, 10000\}$ as shown in Fig. 6a. We see from Fig. 6a that the normalized throughput tends to the ideal threshold curve for the SISO case as the frequency diversity order N_{fd} increases. The OTA throughput curves in Fig. 6a cross the threshold (black line) at different levels corresponding to the probability of detection $PoD(1)$ as defined in (11). These levels define on

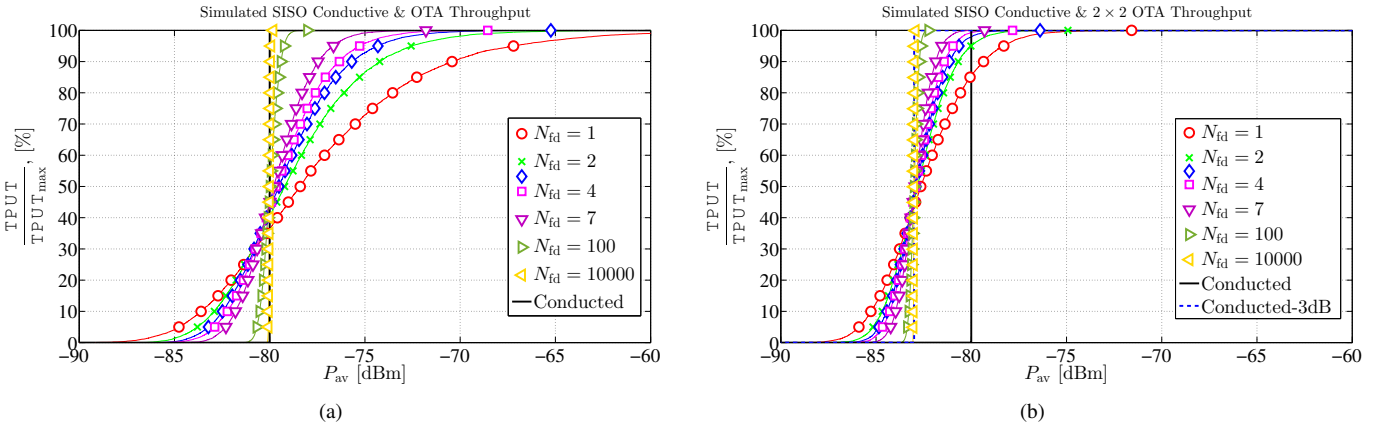


Fig. 6. Modeled conducted throughput and simulated OTA throughput for different orders of frequency diversity ($N_{\text{fld}} = 1, 2, 3, 4, 7, 100, 10000$) for SISO and 2×2 MIMO in diversity mode are depicted in (a) and (b), respectively.

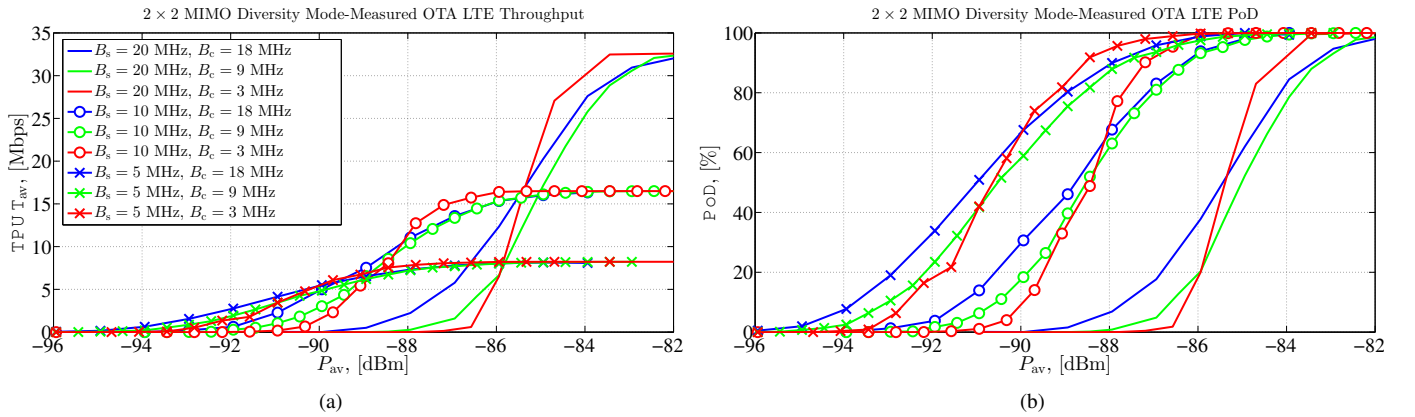


Fig. 7. (a) Measured OTA throughput and (b) corresponding probability of detection of 2×2 MIMO LTE device in diversity mode for different channel coherence bandwidths ($B_c = 3, 9, 18$ MHz) and LTE system bandwidths ($B_s = 20, 10, 5$ MHz).

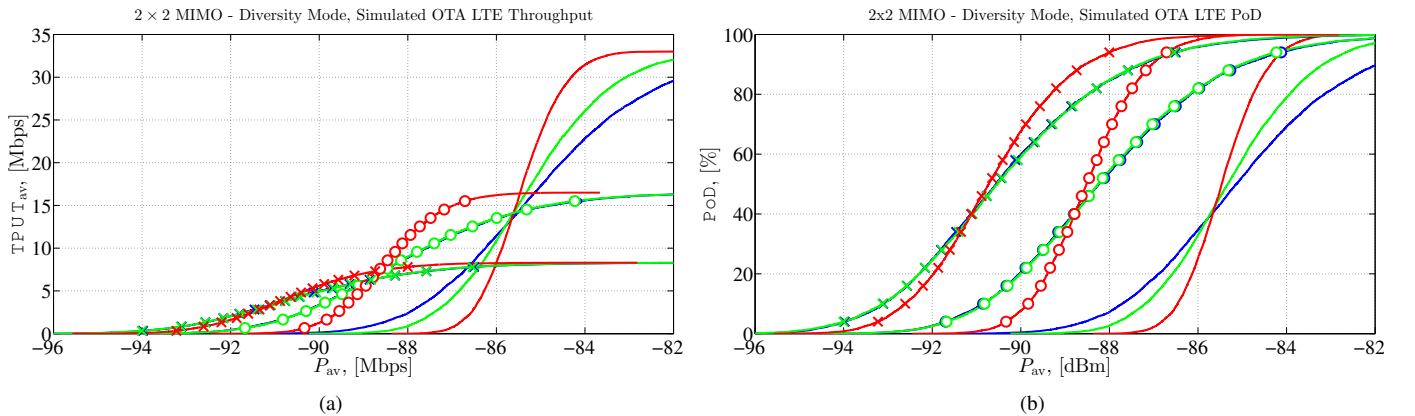


Fig. 8. (a) Simulated OTA throughput and (b) corresponding probability of detection of 2×2 MIMO LTE device in diversity mode for different channel coherence bandwidths ($B_c = 3, 9, 18$ MHz) and LTE system bandwidths ($B_s = 20, 10, 5$ MHz). Same legend as in Fig. 7 applies.

a measured OTA throughput curve, the threshold power level corresponding to the conducted measurements of the DUT. Thus, if we know N_{fld} , we can read the corresponding TIS of the DUT receiver directly from the OTA throughput curve of a SISO system with OFDM. The $\text{PoD}(1)$ values are listed in Table I.

Corresponding results for an ideal 2×2 MIMO system with transmit diversity and receive diversity (i.e., a single bitstream

case) are shown in Fig. 6b. As can be seen, there is a 3 dB array gain in RIMP when compared to a SISO system depicted in Fig. 6a. Thus the TIS obtained for the MIMO case is 3 dB lower than the SISO case under the same conditions are predicted by our models according to (9) and (6), respectively.

The measured LTE DUT throughput v.s. average received power curves are shown in Fig. 7 (see [16], [17] for additional results); corresponding simulated data is shown in Fig. 8.

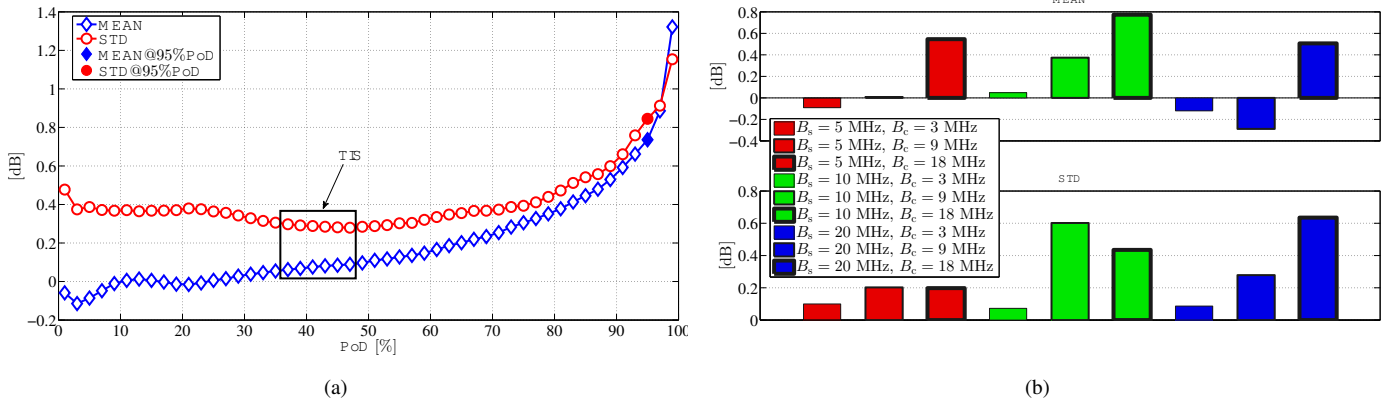


Fig. 9. (a) Mean (MEAN) and standard deviation (STD) of the difference between the simulated and measured power in dB at different PoD levels and (b) Mean (MEAN) and standard deviation (STD) of the difference between the simulated and measured power in dB for the 9 different combinations of system bandwidth and coherence bandwidth. The comparison pertains data presented in Fig. 7b and Fig. 8b.

TABLE II. Estimated & measured TIS for SISO in flat fading & frequency selective fading

B_s , [MHz]	5	10	20	5	10	20	5	10	20
B_c , [MHz]	3	3	3	9	9	9	18	18	18
N_{fd}	2	4	7	1	1	2	1	1	1
σ , [ns]	210	210	210	60	60	60	30	30	30
P_{th} , [dBm]	-89.0	-86.7	-83.4	-89.0	-86.7	-83.4	-89.0	-86.7	-83.4
PoD(1), [%]	40.0	43.0	45.5	36.0	36.0	40.0	36.0	36.0	36.0
$\hat{T}IS$, [dBm] (11)	-87.2	-85.0	-81.4	-86.7	-84.7	-81.3	-89.2	-86.6	-83.2
TIS, [dBm] (8)	-85.39	-84.23	-80.89	-85.77	-84.40	-80.66	-87.68	-86.11	-82.67
Discrepancy, [dB]	1.81	0.77	0.51	0.93	0.27	0.64	1.52	0.49	0.53

TABLE III. Estimated & measured TIS for 2×2 MIMO-diversity mode in flat-fading & frequency selective-fading channels

B_s , [MHz]	5	10	20	5	10	20	5	10	20
B_c , [MHz]	3	3	3	9	9	9	18	18	18
N_{fd}	2	4	7	1	1	2	1	1	1
σ , [ns]	210	210	210	60	60	60	30	30	30
P_{th} , [dBm]	-88.8	-86.5	-83.1	-88.8	-86.5	-83.1	-88.8	-86.5	-83.1
PoD(1), [%]	45.2	47.2	48.0	43.5	43.5	45.2	43.5	43.5	43.5
$\hat{T}IS$, [dBm] (11)	-90.9	-88.6	-85.5	-90.7	-88.4	-85.0	-91.4	-89.1	-85.8
TIS, [dBm] (8)	-89.01	-87.84	-84.78	-88.85	-87.59	-84.42	-90.56	-89.41	-85.58
Discrepancy, [dB]	1.89	0.76	0.72	1.84	0.79	0.58	1.84	-0.31	0.22

As we can see, both measured and simulated plots show very similar behavior. We see that the available maximum throughput increases when the system bandwidth increases, and we need to increase the average power to achieve it, as expected (compare to conducted throughput measurement shown in Fig. 2). This is the received power on an antenna with 100% radiation efficiency when it is averaged over the stirring cycle. Therefore, to increase the average power we must increase the transmit power into the chamber by the base station emulator. For each system bandwidth we have plotted three throughput curves. We see that the curves for the smallest coherence bandwidths are the steepest curves, and that these curves approach the maximum throughput faster when the average power increases. These improvements are due to the frequency diversity gain achieved by OFDM. Thus, with OTA throughput measurements we can clearly see the

improvement of using OFDM, which we could not observe from the standard measurements that provide TIS values alone as shown in Fig. 5. OFDM provides a performance gain that is expected to be larger for smaller coherence bandwidths B_c relative the system bandwidth B_s . Therefore, measured OTA throughput curves are a much better tool than the TIS for quantifying the receiver quality of the device.

Fig. 9 shows a comparison between the measured relative throughput, i.e., PoD shown in Fig. 7b and corresponding simulated data shown in Fig. 8b. The simulated data and the measured data were both interpolated to obtain the mean and standard deviation of the difference between the simulated and measured power in dB at different PoD levels shown in Fig. 9a. The mean and the standard deviation at each PoD level was calculated across the 9 curves shown in Fig. 7b and Fig. 8b. As we can see, both the mean and the standard

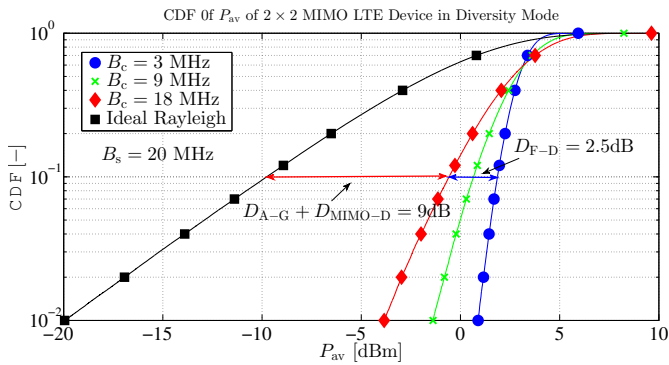


Fig. 10. Simulated 2×2 MIMO OTA LTE throughput in diversity mode for the i.i.d. case presented in terms of the corresponding CDF of the diversity-combined channel, plotted versus the average received power at a reference antenna with 100% efficiency. The different curves show the CDF for different channel coherence bandwidths ($B_c = 3, 9, 18$ MHz) and LTE system bandwidth $B_s = 20$ MHz. The simulated data is the same as presented in Fig. 7.

deviation are below 1dB for $\text{PoD} \leq 95\%$. Moreover, the mean and standard deviation are less than 0.1dB and 0.3dB, respectively, for PoD values corresponding to the levels used in the TIS estimation according to (11) (see Table I). Results, are within the uncertainty limits of the measurements in reverberation chambers, i.e., within 0.5 dB. This is highlighted by the rectangle shown in Fig. 9a. At higher PoD levels, e.g., at the 95% level, the mean and standard deviation are equal to 0.75dB and 0.85dB, respectively. Hence, the simple model used in this paper gives a very good agreement with measurement data, especially for TIS.

Fig. 9b shows the mean and standard deviation calculated across PoD values, i.e., here specifically within 1% – 99%. Results are presented for the three system bandwidths and the three coherence bandwidths considered in both measurements and simulations. As can be seen, both the mean and standard deviation are less than 0.8dB for all cases. The best agreement was obtained for coherence bandwidth $B_c = 3$ MHz resulting in a mean and a standard deviation less than 0.1 dB. In general, the higher the number of uncorrelated OFDM sub-channels, the better the agreement between model and measurements.

D. Throughput measurements and derived diversity gain

The MIMO diversity gains can be observed both as a horizontal shift of the throughput curves, referred to as *array gain* and as a steeper slope of the curve referred to as *diversity gain*. The frequency diversity gains can be observed only by the slope of the throughput curves. In theory, when N_{fd} increases, the slope of the throughput curves representing frequency diversity also increases until the throughput curve is an ideal step function identical to the single-receiver conducted threshold as shown in Fig. 6a and Fig. 6b.

The CDF of the MRC signal has previously been used to quantify the diversity gains in dB [10] and dBR [5]. Fig. 10 shows the simulated data of 2×2 MIMO relative throughput also presented in Fig. 8, but now they are presented in terms of CDFs. The diversity gains in dB are shown relative to a reference curve. It is common to use the Rayleigh curve

as a reference [10]. Then, dBR indicates that the dB value has been obtained relative the Rayleigh CDF. In any case, we must always specify the reference CDF. For example, the total diversity gain $DG = 11.5$ dBR is achieved at 10% CDF-level when measuring throughput with $B_s = 20$ MHz and $B_c = 3$ MHz (dashed blue curve). This large gain relative the ideal Rayleigh curve can be represented as the sum of three terms (14), where $DG_{F-D} = 2.5$ dBR is the frequency diversity gain compared to the same 2×2 MIMO system in a flat fading Rayleigh channel ($N_{fd} = 1$), $DG_{A-G} = 3$ dB results from the array gain $N_r = 2$ and $DG_{MIMO-D} = 6$ dB is the MIMO diversity since 4 MIMO links are subject to MRC. The simulated i.i.d. values of MIMO diversity gains and OFDM frequency diversity gain when CDF = 10% for both SISO and 2×2 MIMO systems are tabulated in Table I.

V. COMPARISON OF THE STANDARD AND THE THROUGHPUT-BASED TIS ESTIMATION

The TIS obtained using the standard measurement procedure and the TIS obtained from throughput measurement for the LTE device are shown in Table II and Table III, for SISO and 2×2 MIMO OFDM systems, respectively. Results are presented for system bandwidths 5, 10, and 20 MHz, for various values of B_s and B_c . As can be seen the agreement between simulated and measured TIS values is good. Moreover, the standard TIS measurement procedure is very time-consuming because we have to read the $P_{av,n}$ value at 800 different stirrer positions in the chamber to achieve good accuracy. On the other hand, the TIS estimated from OTA throughput measurements is obtained directly after one measurement including one search for the $\text{PoD}(1)$ -level of the throughput.

Tables II and III show the threshold power P_{th} read at 50%-level of measured conducted throughput, the estimated TIS from measured OTA throughput curves, and the measured TIS values for different LTE system bandwidths and different coherence bandwidths. For a fixed threshold the TIS value becomes 3 dB better with 2×2 MIMO compared to a SISO system which is due to the MIMO array gain. Further, the threshold value changes by approximately 3 dB when changing system bandwidth from 20 MHz to 10 MHz and by 3 dB more when reducing system bandwidth to 5 MHz. The OTA throughput is measured using the same measurement setup as TIS and includes the effect of antenna efficiency, correlation, noise coupling, and other non-ideal behaviors in similar way as for TIS. There are discrepancies between the estimated and measured TIS values tabulated in Tables II and III.

It should be noted that this discrepancy is smaller than 1 dB for all cases except when $B_s = 5$ MHz. We can expect this from looking at the red 5 MHz curve in Fig. 2 because it has the largest deviation from an ideal threshold by showing a shoulder. The specific reason for this is not known; however a malfunctioning of the device at the narrower bandwidth cannot be discarded. It should be noted that a somewhat weaker effect is also observed for $B_s = 10$ MHz in Fig. 2.

While looking at the discrepancies in Table II and Table III, we should keep in our minds that our TIS estimation is

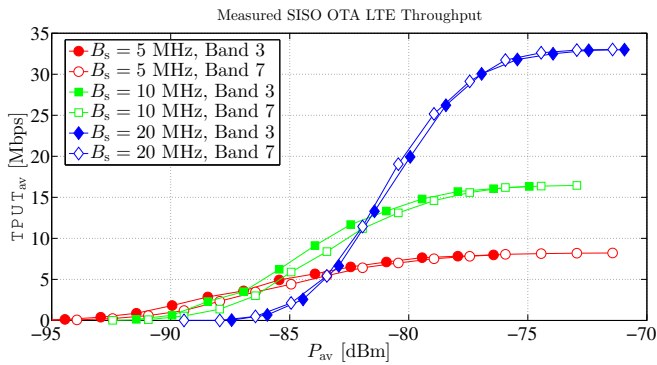


Fig. 11. Measured OTA LTE throughput for SISO system in band 3 and band 7 for different LTE system bandwidths ($B_s = 5, 10, 20$ MHz) and coherence bandwidth $B_c = 9$ MHz.

TABLE IV. Conducted receiver sensitivity obtained from measured throughput in AWGN channel

B_s , [MHz]	5	10	20
$P_{th}@50\%$, [dBm]	-89.0	-86.7	-83.4
$P_{th}@90\%$, [dBm]	-87.7	-86.2	-82.9
$P_{th}@99\%$, [dBm]	-87.1	-85.8	-82.2
$P_{th}@100\%/P_{th}@0\%$, [dB]	3.00	1.50	1.15

based on using the ideal threshold receiver. The theoretical throughput jumps from 0% to 100% over a change in power of 0 dB. The actual DUT which we have chosen for our study has a non-ideal threshold, and we have shown this in Table IV by giving the power levels at three different values of the throughput: 50%, 90% and 99%. These values are device specific and depend very much on the hardware design as well as the algorithms included in the DUT. They could also depend on the quality of the communication test instrument used as base station emulator.

Table IV shows that we have the largest errors in the determination of the threshold when the system bandwidth is 5 MHz. For 10 and 20 MHz system bandwidths, the thresholds are better and they show also the expected 3 dB difference when the bandwidth is doubled.

VI. ADDITIONAL RESULTS WITH DISCUSSION

We have also checked how the throughput and TIS values change for different LTE frequency bands. The following results show the OTA throughput of the same device measured in band 3 (1.8 GHz) and band 7 (2.6 GHz). The throughput results are presented in Fig. 11 and TIS is compared in Table V.

The measured throughput curves in both bands follow each other very well as seen in Fig. 11. Note that this is device specific behavior and there could be a device with different results in different frequency bands. The measured TIS values of the same SISO system with the same measurement settings as in Fig. 11 are presented in Table V. The measured TIS values in two different bands, i.e., bands 3 and 7 are very close to each other except at a system bandwidth of 5 MHz which could very well be explained by the non-ideal threshold at 5 MHz system bandwidth as seen in Fig. 2.

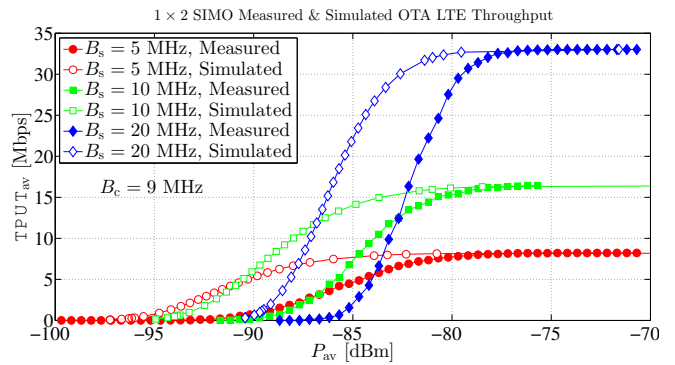


Fig. 12. Measured and simulated OTA LTE throughput for 1×2 SIMO system in band 7 with externally connected antenna for different LTE system bandwidths ($B_s = 5, 10, 20$ MHz) and coherence bandwidth $B_c = 9$ MHz. The measured results are for lossy antennas with efficiency of -4 dB while simulated results are for antennas with efficiency 0 dB.

TABLE V. Comparison of measured TIS (see (8)) for SISO at LTE band 3 & band 7

B_s , [MHz]	5	10	20	5	10	20
B_c , [MHz]	3	3	3	9	9	9
N_{fd}	2	4	7	1	1	2
σ , [ns]	210	210	210	60	60	60
TIS, [dBm]	-89.0	-87.8	-84.8	-88.9	-87.6	-84.4

Finally, we also measured the OTA throughput of the same DUT by using its internal lossy antennas, and we compared them with the simulated results. In all previously shown measured results we used externally connected antennas with high efficiency (i.e., close to 0 dB). In Fig. 12 the throughput of a DUT in 1×2 SIMO configuration, measured using its internal lossy antennas is compared to simulated 1×2 SIMO with 100% efficient antennas. The degradation is 4 dB and this is attributed to the poor embedded radiation efficiencies of the built-in antennas in the device.

As a final remark we can say that, the current work is limited to SISO and MIMO with single-bitstream but can be further extended for multiple bitstreams including cases for which the channel state information is known at the transmitting side. Some works on multiple bitstream measurements and modeling in reverberation chambers have already been published [24]-[29].

VII. DISCUSSION AND CONCLUSIONS

We have studied the receiver sensitivity of LTE devices quantified by the TIS, i.e., the Total Isotropic Sensitivity, for the SISO and the 2×2 MIMO cases when receiving a single bitstream in RIMP environments. The proposed approach is based on the threshold receiver model applied to MIMO OFDM systems operating according to the LTE standard. Based on the analysis provided in this paper we observed that the theoretical throughput curves produced by the model are in good agreement with the measured curves, provided the time delay spread is known and the antenna ports are uncoupled and have equal embedded radiation efficiencies. The estimated TIS shows a small estimation error computed over all the

considered combinations of bandwidths, delay spread of the RIMP channel, etc. The obtained standard deviation and mean of the error equal to 0.1 dB and 0.3 dB, respectively, at the 50% throughput level (or equally the 0.5 probability level at the Probability of Detection (PoD) curves) while at the 95% throughput level the standard deviation and the mean of the error was estimated to 0.75dB and 0.85dB, respectively.

In addition to the very good accuracy, the proposed method demonstrates that for uncoupled MIMO antenna ports (i.e., the i.i.d. case), the TIS can be estimated from one single throughput measurement during continuous fading. This takes less time than performing the standard TIS procedure, which requires several 100 times longer time. This improvement becomes apparent from the fact that the instantaneous throughput curve at any position in a reverberation chamber shows the same step-function behavior as the measured conducted throughput curve, but at another power level, as a result of the flat-fading behavior of OFDM channels. The TIS measured according to the standard approach will theoretically not be affected by the OFDM function, provided the embedded radiation efficiencies on the antenna ports do not vary over the system bandwidth.

The diversity gain of a MIMO enabled wireless device measured in a RIMP environment can also be modeled by the same threshold receiver model as for the TIS. The shift of the throughput curves and their slopes can be then explained by the number of MRC spatial diversity channels and the OFDM diversity channels explained by simple equations directly relating throughput and received power. Indeed, the throughput curves contain a more comprehensive and reliable information on receiver quality than the TIS value alone. Therefore, it is much better to characterize receiver sensitivity in terms of OTA throughput for LTE devices. In practice, the calibrated received power relative a reference antenna with 100% radiation efficiency, e.g., corresponding to 90% or 95% throughput levels are deduced from the measured throughput curves for the desired specific system configurations and time delay spreads of the RIMP channels. Comparing these levels we can directly interpret the difference in terms of contributions from the conducted threshold level at the receiver (corresponding to the classical TIS value), embedded radiation efficiency (shift of the throughput curve), array gain (shift of the curve), and diversity gain (steeper slope of the curve).

The throughput curves presented here represent a PoD of the single bitstream over all the environment-realizations during the continuous stirring in the reverberation chamber. Thereby it is possible to generalize the continuous throughput measurement approach to a step-by-step procedure over stationary stirrer positions. Then, we can even consider characterizing other statistical variations by using such a PoD, e.g. different stationary user locations or user practices. *In reverberation chambers we have PoDs in RIMP, but we can also use the same threshold receiver approach to determine the PoD in other types of environments.*

ACKNOWLEDGMENT

The authors thank Mats Kristoffersen, and Magnus Franzén at Bluetest AB for their support to perform measurements to validate theoretical results. The authors also thank Prof. Giuseppe Durisi, Prof. Erik Ström at Chalmers and Prof. Jan Carlsson at SP Technical Research Institute of Sweden for discussions.

REFERENCES

- [1] CTIA Certification, Test Plan for Mobile Station Over the Air Performance, "Method of Measurement for Radiated RF Power and Receiver Performance," Revision Number 3.1, January 2011.
- [2] 3GPP TS 34.114 V11.1.0 (2012-06), "User equipment (UE) / mobile station (MS) over the air (OTA) antenna performance," Conformance testing (Release 11).
- [3] 3GPP TS 36.521-1 V11.2.0 (2013-10), "Evolved Universal Terrestrial Radio Access (E-UTRA); User Equipment (UE) conformance specification; Radio transmission and reception; Part 1: Conformance testing
- [4] P.-S. Kildal and K. Rosengren, "Correlation and capacity of MIMO systems and mutual coupling, radiation efficiency, and diversity gain of their antennas: simulations and measurements in a reverberation chamber," *Communications Magazine, IEEE*, vol. 42, pp. 104-112, 2004.
- [5] P.-S. Kildal, C. Orlenius, and J. Carlsson, "OTA Testing in Multipath of Antennas and Wireless Devices With MIMO and OFDM," *Proceedings of the IEEE*, vol. 100, pp. 2145-2157, 2012.
- [6] A. A. Glazunov, V. M. Kolmonen, and T. Laitinen, "MIMO over-the-air testing, in LTE-Advanced and Next Generation Wireless Networks: Channel Modelling and Propagation. Hoboken, NJ, USA: Wiley, 2012, pp. 411-441.
- [7] N. Serafimov, P.-S. Kildal, and T. Bolin, "Comparison between radiation efficiencies of phone antennas and radiated power of mobile phones measured in anechoic chambers and reverberation chamber," in *Antennas and Propagation Society International Symposium*, 2002. IEEE, 2002, pp. 478-481 vol.2.
- [8] C. Orlenius, P.-S. Kildal, and G. Poilasne, "Measurements of total isotropic sensitivity and average fading sensitivity of CDMA phones in reverberation chamber," in *Antennas and Propagation Society International Symposium*, 2005 IEEE, 2005, pp. 409-412 Vol. 1A.
- [9] N. Olano, C. Orlenius, K. Ishimiya, and Y. Zhinong, "WLAN MIMO throughput test in reverberation chamber," in *Antennas and Propagation Society International Symposium*, 2008 (AP-S 2008). IEEE, 2008, pp. 1-4.
- [10] P.-S. Kildal, K. Rosengren, J. Byun, and J. Lee, "Definition of effective diversity gain and how to measure it in a reverberation chamber," *Microwave and Optical Technology Letters*, vol. 34, pp. 56-59, 2002.
- [11] K. Rosengren and P.-S. Kildal, "Radiation efficiency, correlation, diversity gain and capacity of a six-monopole antenna array for a MIMO system: theory, simulation and measurement in reverberation chamber," *Microwaves, Antennas and Propagation, IEE Proceedings -*, vol. 152, pp. 7-16, 2005.
- [12] A. M. Asghar, M. Malick, M. Karlsson, and A. Hussain, "A multiwide-band planar monopole antenna for 4G devices," *Microwave and Optical Technology Letters*, vol. 55, pp. 589-593, 2013.
- [13] H. Raza, J. Yang, and A. Hussain, "Measurement of Radiation Efficiency of Multiport Antennas With Feeding Network Corrections," *Antennas and Wireless Propagation Letters, IEEE*, vol. 11, pp. 89-92, 2012.
- [14] X. Chen, P.-S. Kildal, J. Carlsson, and J. Yang, "MRC Diversity and MIMO Capacity Evaluations of Multi-Port Antennas Using Reverberation Chamber and Anechoic Chamber," *IEEE Transactions on Antennas and Propagation*, vol. 61, pp. 917-926, 2013.
- [15] P.-S. Kildal, X. Chen, C. Orlenius, M. Franzen, and C. S. L. Patane, "Characterization of Reverberation Chambers for OTA Measurements of Wireless Devices: Physical Formulations of Channel Matrix and New Uncertainty Formula," *IEEE Transactions on Antennas and Propagation*, vol. 60, pp. 3875-3891, 2012.
- [16] A. Hussain and P.-S. Kildal, "Study of OTA throughput of LTE terminals for different system bandwidths and coherence bandwidths," in *7th European Conference on Antennas and Propagation (EuCAP)*, 2013 2013, pp. 312-314.
- [17] P.-S. Kildal, A. Hussain, X. Chen, C. Orlenius, A. Skarbratt, J. Asberg, T. Svensson, and T. Eriksson, "Threshold Receiver Model for Throughput of Wireless Devices With MIMO and Frequency Diversity Measured in Reverberation Chamber," *Antennas and Wireless Propagation Letters, IEEE*, vol. 10, pp. 1201-1204, 2011.

- [18] A. Hussain, P.-S. Kildal, U. Carlberg, and J. Carlsson, "Diversity gains of multipoint mobile terminals in multipath for talk positions on both sides of the head," in *7th European Conference on Antennas and Propagation (EuCAP)*, 2013, pp. 863-866.
- [19] E. Dahlman, S. Parkvall, and J. Sködl, *4G LTE/LTE Advanced for Mobile Broadband*, Academic Press, 2011.
- [20] T. K. Y. Lo, "Maximum ratio transmission, *IEEE Trans. Commun.*, vol. 47, pp. 1458-1461, Oct. 1999.
- [21] X. Chen, P.-S. Kildal, C. Orlenius, and J. Carlsson, "Channel Sounding of Loaded Reverberation Chamber for Over-the-Air Testing of Wireless Devices: Coherence Bandwidth Versus Average Mode Bandwidth and Delay Spread," *Antennas and Wireless Propagation Letters, IEEE*, vol. 8, pp. 678-681, 2009. See also correction in Vol. 12, 2013.
- [22] G. De la Roche, A. A. Glazunov, B. Allen, *LTE-Advanced and Next Generation Wireless Networks: Channel Modelling and Propagation*, John Wiley and Sons, Chichester UK, 2013.
- [23] C. L. Holloway, D. A. Hill, J. M. Ladbury, P. F. Wilson, G. Koepke, and J. Coder, "On the use of reverberation chambers to simulate a Rician radio environment for the testing of wireless devices, *IEEE Trans. Antennas Propag.*, vol. 54, pp. 3167-3177, 2006.
- [24] P.-S. Kildal, A. Hussain, G. Durisi, C. Orlenius, and A. Skarbratt, "LTE MIMO multiplexing performance measured in reverberation chamber and accurate simple theory," in *Antennas and Propagation (EUCAP)*, 2012 6th European Conference on, 2012, pp. 2299-2302.
- [25] X. Chen, P.-S. Kildal, and M. Gustafsson, "Characterization of Implemented Algorithm for MIMO Spatial Multiplexing in Reverberation Chamber," *Antennas and Propagation, IEEE Transactions on*, vol. 61, pp. 4400-4404, 2013.
- [26] D. A. Hill, M. T. Ma, A. R. Ondrejka, B. F. Riddle, M. L. Crawford, and R. T. Johnk, "Aperture excitation of electrically large, lossy cavities," *Electromagnetic Compatibility, IEEE Transactions on*, vol. 36, pp. 169-178, 1994.
- [27] B. Jinkyu, L. Young Ju, K. Yongsup, and A. S. Kim, "Calculation of total isotropic sensitivity considering digital harmonic noise of mobile phone," in *Antennas and Propagation Society International Symposium, 2009. APSURSI '09. IEEE*, 2009, pp. 1-4.
- [28] P. J. Bevelacqua. (2011). *The Antenna Theory Website*. Available: <http://www.antenna-theory.com/definitions/tis.php>
- [29] X. Chen, B. T. Einarsson, and P.-S. Kildal, "Improved MIMO Throughput with Inverse Power Allocation Study using USRP Measurement in Reverberation Chamber," *IEEE Antennas and Wireless Propagation Letters (AWPL)*, vol. 13, pp. 1494-1496, 2014.